ATLAS NOTE

ATLAS-CONF-2012-157

November 12, 2012

Measurement of the combined WW and WZ production cross section in the semileptonic final state in proton-proton collisions at $\sqrt{s} = 7$ TeV with the ATLAS detector

The ATLAS Collaboration

ATLAS-CONF-2012-157
13 November 2012

Abstract

A study of WW/WZ production in the semileptonic final state using a 4.7 ± 0.2 fb^{-1} sample of proton-proton collisions at $\sqrt{s} = 7$ TeV recorded with the ATLAS detector at the Large Hadron Collider in 2011 is presented. The cross section is measured in the $WW/WZ \to \ell\nu q\bar{q}'$ decay channel where the lepton can be a muon or an electron. The measured cross section is $\sigma(WW + WZ) = 72 \pm 9$ (stat.) $\pm$ 15 (syst.) $\pm$ 13 (MC stat.) pb, consistent with the Standard Model expectation of 63.4 ± 2.6 pb.

1 Introduction

The production of gauge-boson pairs in pp collisions, such as WW, provides an important test of the electroweak sector of the Standard Model (SM) and represents a major background for SM Higgs boson production and possible new physics processes. Furthermore, deviations of the cross section from predictions could arise from anomalous triple gauge boson interactions [1] or from new resonances decaying to vector bosons. The WW and WZ production cross sections in pp collisions, calculated at next-to-leading-order (NLO), are $\sigma(WW) = 44.9 \pm 2.2$ pb and $\sigma(WZ) = 18.5 \pm 1.3$ pb [2, 3]. The cross sections for WW and WZ production at the LHC have only been measured in fully leptonic final states [4–7]. Semileptonic final states suffer from larger backgrounds from W/Z boson production in association with jets, but benefit from a significantly larger branching ratio relative to the fully leptonic state and thus represent an important complementary measurement. The production cross section of WW and WZ in the semileptonic final state have been measured [8, 9] in $p\bar{p}$ collisions at the Tevatron hadron collider by both CDF and DØ and recently, in pp collisions, by CMS [10].

This note describes a measurement of the WW and WZ boson production cross section in the semileptonic decay mode, where one of the W bosons decays into an electron or a muon and their corresponding neutrino, and the other W or the Z decays into a quark and anti-quark. This results in an experimental signature of an electron or muon, two jets, and missing transverse energy ($E_{\mathrm{T}}^{\mathrm{miss}}$). Since experimentally the reconstructed di-jet mass resolution is insufficient to distinguish W bosons from Z bosons, the WW and WZ cross sections are measured together. The measurement is performed with a dataset corresponding to an integrated luminosity of 4.7 ± 0.2 fb^{-1} [11] of data collected by the ATLAS detector at the LHC in 2011.

2 ATLAS Detector

The ATLAS experiment [12] uses a multipurpose particle physics detector with forward-backward symmetric cylindrical geometry[a] covering the pseudorapidity range $|\eta| < 2.5$ for track and $|\eta| < 4.9$ for jet measurements. The inner tracking detector consists of a silicon pixel detector, a silicon microstrip detector, and a straw tube transition radiation tracker. The inner tracker is surrounded by a thin superconducting solenoid, providing a 2 T magnetic field, and by a high-granularity liquid-argon (LAr) sampling electromagnetic calorimeter. A steel and scintillator tile calorimeter provides hadronic coverage in the central rapidity range. The end-cap and forward regions are instrumented with LAr calorimetry for both electromagnetic and hadronic measurements. The muon spectrometer surrounds the calorimeters and consists of three large superconducting toroids, each with eight coils, a system of precision tracking chambers, and detectors for triggering.

3 Data and Simulated Event Samples

Events were collected using a three-level trigger by requiring the presence of an electron or muon above a certain transverse momentum (p_{T}) threshold. The p_{T} threshold for the single-muon trigger was set to 18 GeV, while for electrons it was set to 20 GeV for the early part of the run and was later raised to 22 GeV when the instantaneous luminosity of the LHC increased. Simulated event samples are used to model both the signal and all the background processes, except for the multijet background, which

[a] ATLAS uses a right-handed coordinate system with its origin at the nominal interaction point (IP) in the center of the detector and the z-axis coinciding with the axis of the beam pipe. The x-axis points from the IP to the center of the LHC ring, and the y-axis points upward. Cylindrical coordinates (r, ϕ) are used in the transverse plane, ϕ being the azimuthal angle around the beam pipe. The pseudorapidity η is defined in terms of the polar angle θ as $\eta = -\ln[\tan(\theta/2)]$.

is estimated using a data-driven procedure. The response of the ATLAS detector is simulated [13] using GEANT4 [14]. The dominant background to the $WW/WZ \to \ell\nu q\bar{q}'$ process is vector boson W/Z production in association with jets.

The vector boson processes, W/Z+jets, are generated using ALPGEN v2.13 [15] with CTEQ6L1 [16] for the parton distribution functions (PDFs), interfaced to HERWIG v6.510 [17] and JIMMY v4.31 [18]. Exclusive samples with zero to four additional partons (np with $n = 0 - 4$) and an inclusive sample with five or more additional partons (np with $n = 5$) are used. The cross sections are computed using the ALPGEN cross sections scaled so that the sum of the np sample cross sections is equal to the next-to-next-to-leading-order (NNLO) inclusive cross section times branching fraction for a single lepton species: $\sigma(W \to \ell\nu) = 10.46 \pm 0.42$ nb and $\sigma(Z/\gamma^* \to \ell\ell) = 1.070 \pm 0.054$ nb for invariant masses of the two leptons ($m_{\ell\ell}$) > 40 GeV [19, 20]. Production of W and Z plus heavy flavor jets is also modeled using the ALPGEN+HERWIG+JIMMY generator combination described above. Additional samples for cross checks are generated using SHERPA 1.1.3 [21] with PDF set CTEQ6L1, and PYTHIA 6.421 [22] with PDF MRST 2007 LO* [23]. Samples of $t\bar{t}$ events are produced using MC@NLO v3.41 [3] and POWHEG 1.01 patch 4 [24] with PDF CTEQ6.6M [25] interfaced to HERWIG for parton showering. Cross sections are scaled to the next-to-next-to-leading-log (NNLL) prediction of 167^{+16}_{-18} pb [26]. Single top events are generated using MC@NLO with cross sections of 4.6 pb, 64.6 pb, and 16.1 pb for the s–, t–, and tW–channels respectively. Their uncertainties are of the order of ±5% [27–29]. Samples of $t\bar{t}$ generated with AcerMC [30] are also considered for systematic uncertainty studies.

Diboson events are generated using HERWIG for the nominal samples and using PYTHIA [22] for systematic studies. The diboson samples are normalized to the next-to-leading order (NLO) cross sections of 44.9 ± 2.2 pb, 18.5 ± 1.3 pb, and 5.96 ± 0.3 pb for WW, WZ, and ZZ ($m_{\ell\ell} > 60$ GeV) respectively. The nominal values of the diboson NLO cross sections have been estimated using MCFM [31] with MSTW2008NLO [32] PDF. The uncertainties are evaluated by the combined scale (factorization and normalization) and 90% CL. PDF+α_s uncertainties. The combined PDF+α_s uncertainties are estimated following the procedure of Ref. [33].

The $W\gamma$ process, which has been generated with PYTHIA, gives a small contribution to the background.

Each simulated sample is divided into subsamples that reflect the changes in the data-taking conditions in 2011. The average number of interactions per bunch crossing, $\langle\mu\rangle$, increased throughout 2011 with the instantaneous luminosity, and reached a maximum of 17. Particles produced in multiple interactions, either coincident with the event of interest or in neighbouring bunch crossings, are referred to as 'pile-up' and are included in the simulation. The number of extra interactions in simulated events is adjusted according to the measured $\langle\mu\rangle$ distribution in each data-taking period.

4 Event Reconstruction and Signal Selection

Events are required to pass the single lepton trigger and, in order to remove non-collision backgrounds, are required to contain a primary vertex reconstructed from at least three charged-particle tracks, each with $p_{\mathrm{T}} > 400$ MeV. In events where multiple collision vertices are reconstructed, the vertex with the largest Σp_{T}^2 of the associated tracks is defined as the primary vertex.

4.1 Object Reconstruction and Selection

The WW/WZ decays are identified by requiring one high-p_{T} lepton (electron or muon), missing transverse energy, and two jets.

Electron candidates are formed by matching electromagnetic calorimeter clusters to tracks reconstructed in the inner detector [34]. The transverse energy (E_{T}), calculated from the cluster energy and

the track direction, must be greater than 25 GeV, in order to be on the trigger plateau. Candidates are accepted if they lie in the region $|\eta| < 2.47$, excluding the crack region between the barrel and endcap electromagnetic calorimeters, $1.37 < |\eta| < 1.52$. The lateral and transverse shapes of the energy cluster must be consistent with those of an electromagnetic shower. For the electron-candidate track, the ratio of the transverse impact parameter (d_0) to its uncertainty (the d_0 significance), must be smaller than 10. The longitudinal impact parameter z_0 must have an absolute value less than 1 mm. To ensure isolation, both calorimetric and tracking criteria are applied. The total calorimeter E_{T} in a cone of $\Delta R = 0.3$ [b] around the electron candidate, excluding E_{T} of the candidate itself, must be less than 14% of the electron E_{T} value. Meanwhile, the scalar sum of the p_{T} values of the tracks within $\Delta R = 0.3$ of the electron candidate must be less than 13% of the electron p_{T} value. The calorimeter response is corrected for the additional energy deposited by pile-up.

Muon candidates are identified [35] by matching tracks reconstructed in the muon spectrometer to tracks reconstructed in the inner detector. The momentum of the combined muon track is calculated from the momenta of the two tracks corrected for the energy loss in the calorimeter. Muon candidates must satisfy $p_{\mathrm{T}} > 25$ GeV and $|\eta| < 2.4$. The p_{T} threshold is chosen to be well within the plateau of the trigger efficiency. Muon candidates must also be consistent with originating from the primary vertex, in order to reject muons from cosmic ray interactions and to reduce background from heavy flavor decays. Specifically, we require that the d_0 significance be less than 3 and that $|z_0|$ be less than 1 mm. To reduce misidentification and improve on the muon momentum resolution, requirements on the minimum number of hits in the various detectors are applied to the muon tracks. Isolated muons are selected with a requirement that the scalar sum of p_{T} of the tracks within $\Delta R = 0.3$ of the muon be less than 15% of the muon p_{T} and that the total calorimeter E_{T} in a cone of $\Delta R = 0.3$ around the muon candidate be less than 14% of the muon p_{T}.

Jets are reconstructed from three dimensional clusters of energy, defined at the electromagnetic scale, using the anti-k_t algorithm [36] with radius parameter $R = 0.4$ and full four-momenta recombination. The reconstructed jets are then calibrated using Monte Carlo (MC) to the reference generated jet energy [37]. The reference jets used for this jet calibration are obtained by executing the anti-k_t algorithm on the final state generated particles before detector simulation. This definition includes muons from hadronic decays. The applied calibration consists of an average shift (to correct for pile-up) and a multiplicative correction factor, obtained from MC simulation in bins of η and p_{T}. As a last step the calibration is refined by using in-situ measurements that reduce the uncertainty on the jet energy scale.

Jets consistent with being produced from pile-up interactions are identified using the Jet Vertex Fraction variable (JVF). This variable is defined as the ratio between the scalar sum of p_{T} of the tracks associated with the jets and originating from the primary vertex and the scalar sum of p_{T} of all tracks associated with the jet. Jets are selected if they have JVF larger than 75% or if they have no associated track. The efficiency of this cut is 95% up to $|\eta| < 2.5$ and is well modeled by the MC simulation. Jets are required to pass quality criteria and to lie at a distance $\Delta\mathrm{R} > 0.5$ from well-identified leptons.

The $E_{\mathrm{T}}^{\mathrm{miss}}$ is estimated from reconstructed electrons with $|\eta| < 2.47$, muons with $|\eta| < 2.7$, jets with $|\eta| < 4.9$, and clusters of energy in the calorimeter not included in reconstructed objects with $|\eta| < 4.5$ [38]. The clusters are calibrated to the electromagnetic or the hadronic energy scale according to cluster characteristics. The expected energy deposit of identified muons in the calorimeter is subtracted.

4.2 Selection of WW and WZ candidates

The electron and muon channels are analyzed separately but the selection of the candidates for the leptonically decaying W boson follows a similar strategy for the two channels. Events are required to contain exactly one reconstructed lepton candidate (electron or muon) with $p_T > 25$ GeV. Events with more than

[b] The angular distance ΔR between reconstructed objects is defined as $\Delta R = \sqrt{\Delta\phi^2 + \Delta\eta^2}$.

one well reconstructed and identified lepton are rejected in order to suppress the Z+jets background. Events are required to have $E_{\mathrm{T}}^{\mathrm{miss}} > 30$ GeV in order to account for the presence of the unobserved neutrino from the $W \to \ell\nu$ decay. The transverse mass, m_{T}, is calculated from the lepton transverse momentum and the $E_{\mathrm{T}}^{\mathrm{miss}}$ and is required to be greater than 40 GeV. The $E_{\mathrm{T}}^{\mathrm{miss}}$ and m_{T} cuts highly suppress the multijet background.

Events are required to contain two and only two jets with $|\eta| < 2$ and $p_{\mathrm{T}} > 25$ GeV, and one of these jets must have $p_{\mathrm{T}} > 30$ GeV. These selection criteria strongly suppress the background from top events and improve the signal over background ratio. In order to reduce the multijet background, the azimuthal angular separation between the leading jet and the missing transverse energy direction must fulfill $\Delta\phi(E_{\mathrm{T}}^{\mathrm{miss}}, j_1) > 0.8$. Finally, the angular distances between the two jets must satisfy $\Delta R(j_1, j_2) > 0.7$ and $\Delta\eta(j_1, j_2) < 1.5$.

After applying all selection criteria, 100055 events are found in the electron channel and 103627 in the muon channel.

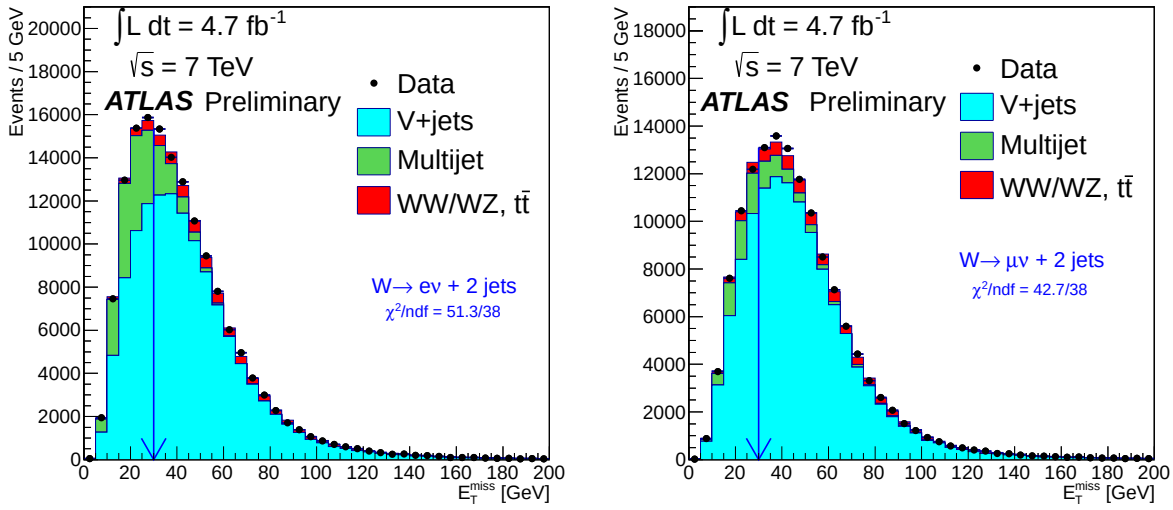

Figure 1: Distributions of $E_{\mathrm{T}}^{\mathrm{miss}}$ for the electron (left) and muon (right) channels. Filled circles show the experimental data and the stacked histograms are SM predictions obtained by fitting the $E_{\mathrm{T}}^{\mathrm{miss}}$ data distribution as explained in the text. The vertical arrow indicates the $E_{\mathrm{T}}^{\mathrm{miss}}$ analysis cut for the signal selection. The values of χ^2/ndf are also shown on the plots.

4.3 Signal and Background Modeling

The SM predictions for signal and background processes are obtained combining results derived from simulated samples and from data-driven techniques. These predictions are used to evaluate the quality of the data/MC modeling. The SM prediction is also used to obtain the expected m_{jj} distribution that is fitted to the observed m_{jj} distribution, as described in Section 6, to extract the WW/WZ production cross section.

The expected shapes of the distributions and production rates for the $t\bar{t}$, single top and diboson samples are obtained from the Monte Carlo simulation. The expected shape for the W + jets and Z + jets (including both light jets and heavy flavor jets) distributions is also obtained from the Monte Carlo simulation. The shape and normalization for the multijet background and the normalization of the W + jets

and Z + jets (including both light jets and heavy flavor jets) contributions are obtained using data-driven methods.

The multijet background originates mostly from events with a semileptonic heavy-flavor decay. In the electron channel, there is also a second component from events where a light-flavor jet is misidentified as an electron. The multijet background is estimated from data since the Monte Carlo simulation does not reliably predict the rate of jets passing the lepton identification. The data-driven method exploits a suitably modified lepton selection to define a control sample dominated by multijet background and with kinematic distributions as close as possible to those of the standard selection. This sample is used to define the shape of the various distributions for the multijet background.

For the muon channel the shape of the multijet background is constructed by applying the muon selection criteria described above, but inverting the transverse impact parameter requirement with respect to the primary vertex by requiring $|d_0/\sigma(d_0)| > 3$. The track must still be within 1 mm of the primary vertex in z. The sample is composed of muons that do not originate from the primary vertex, as expected for muons produced from heavy-flavor decays in jets. For the electron channel the multijet background shape is obtained by applying the electron selection criteria described above, but with relaxed identification criteria to enrich the sample of events with jets that mimic an electron. In both the electron and muon channels, the estimated contributions from all the simulated processes that pass the multijet selection are subtracted from the data-driven template.

The normalizations of the multijet background and W+jets contribution are then assessed from a fit to the $E_{\mathrm{T}}^{\mathrm{miss}}$ spectrum in data over the range $0 < E_{\mathrm{T}}^{\mathrm{miss}} < 100$ GeV. The scale factors from the fit to the $E_{\mathrm{T}}^{\mathrm{miss}}$ distribution are then used to normalize the multijet, W + jets, and Z + jets samples in the SM prediction distributions after applying the appropriate cut on $E_{\mathrm{T}}^{\mathrm{miss}}$. Figure 1 shows the $E_{\mathrm{T}}^{\mathrm{miss}}$ distribution for data after all selection criteria, overlaid with the result of the fit for the electron channel (left) and muon channel (right). The value of the χ^2/ndf for the fit in the electron (muon) channel is 51.3/38 (42.7/38). The fraction of the multijet contribution in the signal region ($E_{\mathrm{T}}^{\mathrm{miss}} > 30$ GeV) is extrapolated and is found to be 5% and 3.8% for electron and muon channel respectively. The correction factor applied to the W/Z+jets processes are 0.98 and 0.95 for the electron and muon channel, respectively.

Table 1 shows the expected number of events for the signal and for each background process after the full selection (including the $E_{\mathrm{T}}^{\mathrm{miss}}$ cut) has been applied . The number of events observed in data, the signal to background ratio and the signal efficiency in the range $60 < m_{jj} < 120$ GeV are also listed.

Data and MC distributions of the main kinematics variables are all in agreement within the systematic uncertainties; a detailed description of the systematic uncertainties is given in Section 5. The $p_{T\,j_1}$, $p_{T\,j_2}$, $\Delta R(j_1, j_2)$, and dijet invariant mass (m_{jj}) distributions summed over the electron and muon channels are shown in Figure 2.

5 Systematic Uncertainties

The effect of systematic uncertainties on both the normalization and the shape of the dijet invariant mass distributions are considered. For each variation of each systematic uncertainty, a template is obtained for the m_{jj} distribution. These templates are used in the fit described in Section 6. Systematic effects from the following sources are taking into account: background normalization, object modeling (jet energy resolution and scale, lepton trigger and reconstruction efficiencies and energy scale), MC modeling, multijet normalization and shape and luminosity.

Background normalization

The systematic uncertainties on the theoretical cross sections used to normalize backgrounds are taken into account. The W/Z+jets cross section is assigned an uncertainty of 20% [20]. The uncertainty is

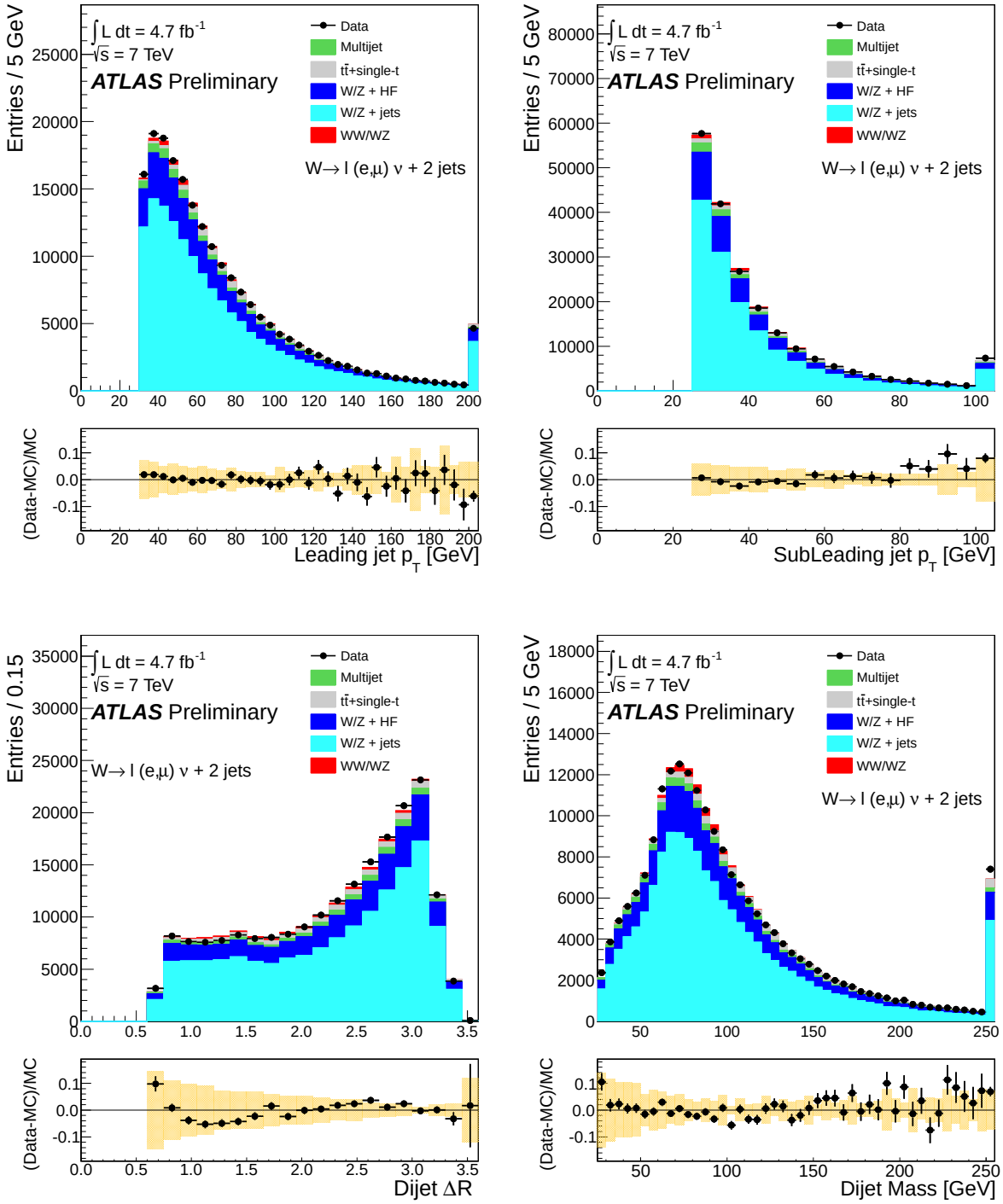

Figure 2: Distributions of the leading (top left) and sub-leading (top right) jet transverse momenta, of their angular distance ΔR (bottom left) and of the di-jet invariant mass distribution of reconstructed $W/Z \rightarrow jj$ candidates (bottom right). The distributions are for the electron and muon channels summed together. Filled circles show the experimental data and the stacked histograms are SM predictions. The rightmost bins include overflow. In each plot, the lower panel displays the fractional difference between the data and the MC expectation. The yellow bands show the JES systematic uncertainty, which dominates.

Process	e	μ
WW	1250 ± 60	1360 ± 70
WZ	276 ± 19	306 ± 21
W + light jets	$(67 \pm 13) \times 10^3$	$(71 \pm 14) \times 10^3$
W/Z + heavy flavor jets	$(19 \pm 4) \times 10^3$	$(20 \pm 4) \times 10^3$
$t\bar{t}$	$(24.8 \pm 2.5) \times 10^2$	$(24.6 \pm 2.5) \times 10^2$
single top	$(13.5 \pm 1.3) \times 10^2$	$(13.7 \pm 1.4) \times 10^2$
multijet	$(50 \pm 15) \times 10^2$	$(39 \pm 12) \times 10^2$
Z + jets	$(35 \pm 7) \times 10^2$	$(32 \pm 6) \times 10^2$
Wγ + ZZ	383 ± 19	464 ± 23
Total SM prediction	$(100 \pm 14) \times 10^3$	$(103 \pm 15) \times 10^3$
Total Data	100055	103627
Signal efficiency for $60 < m_{jj} < 120$ GeV	0.7%	0.9%
Signal to background ratio for $60 < m_{jj} < 120$ GeV	2.6%	2.8%

Table 1: Total number of events in data and expected yields for each process. The multijet and W/Z+jets yields are obtained from the fit to the $E_{\mathrm{T}}^{\mathrm{miss}}$ distribution as explained in Section 4.3. Uncertainties for the expected yields are based on the corresponding cross-section uncertainties. The last two rows list the signal efficiency and signal to background ratio for the two channels.

larger than that one for the inclusive W/Z+jets inclusive cross section since most of the background from this process is composed by W/Z boson plus two or three jets events that are affected by larger cross section uncertainties. The combined $t\bar{t}$ and single top cross section is assigned an uncertainty of 10% [39].

Object Modeling

Systematic uncertainties for the reconstruction and energy calibration of jets, electrons and muons are propagated through the analysis. The main uncertainty arises from the jet energy scale, that includes the effect of pile-up. The jet energy scale and resolution are each varied by their total uncertainties [37] for all simulated samples. The effects of the scale and resolution uncertainties are measured independently. The variations in scale and resolution are also propagated to the $E_{\mathrm{T}}^{\mathrm{miss}}$.

For electrons and muons the efficiencies for reconstruction, isolation and impact-parameter requirements are studied with W, Z and J/ψ samples. Differences between the observed data and simulated samples are corrected. The uncertainties on the correction factors are used to evaluate the systematic uncertainties.

MC generators

Uncertainties for WW and WZ signal events arising from differences in the modeling of the parton shower and hadronization are estimated by changing the models between PYTHIA and HERWIG .

The systematic uncertainties due to the production models of W+jets and Z+jets events are determined by making generator–level comparisons of the yields from samples with varied parameters to the yields from samples with nominal parameter values. This follows the procedures of Ref. [20], and includes variations of the minimum parton p_{T} and the parton-jet matching cone size in the MLM matching scheme [15]. The difference between ALPGEN and SHERPA is also used to estimate the generator modeling systematic uncertainty.

Systematic uncertainties arising from the modeling of the $t\bar{t}$ background are taken into account as well. The largest contributions come from the amount of initial- and final-state radiation (ISR/FSR), estimated using dedicated AcerMC samples interfaced to PYTHIA where parameters controlling the ISR/FSR emission are varied.

Multijet background

Systematic uncertainties on shape and normalization of the multijet backgrounds are determined by using an alternate control sample obtained by reversing the isolation criteria for the electron and muon candidate. The difference in yields and shape between the two methods is used to determine the systematic uncertainty. The yield systematic uncertainty amounts to 30%.

PDF

Uncertainties due to the PDFs are computed using the CT10 eigenvectors and the difference between the CT10 and MSTW2008 [32] PDF sets.

Luminosity

An integrated luminosity uncertainty of 3.9% [11] is applied to the measured cross section.

6 Fitting procedure

The WW/WZ production cross section is extracted by performing a binned maximum-likelihood fit of the observed di-jet invariant mass distribution of reconstructed $W/Z \to jj$ candidates. The fit determines the value of the ratio (μ) between the measured and the NLO SM cross section. From this ratio the measured cross section is obtained using the NLO theoretical cross section values discussed above.

The fit is done considering, in each channel, four components: $WW + WZ$ signal, W/Z+jets (again including both light and heavy flavor jets), top (including both $t\bar{t}$ and single-top production), and multijet background. The contribution of each component to the di-jet invariant mass distribution is described by a m_{jj} template (Figure 3) obtained by normalizing to unit area the di-jet invariant mass distribution of each process derived from MC or from a data-driven procedure.

The fit is done simultaneously for the electron and muon channels, and both the background-only and signal-plus-background hypotheses are tested. Systematic uncertainties for the normalization and shape of signal and background are accounted for by introducing "nuisance" parameters into the fit. In this approach, the normalization of the signal or background component k is given by $N_k = N_{k,\mathrm{nom}} \prod_j \eta_{jk}$, where $N_{k,\mathrm{nom}}$ is the nominal normalization of component k and the product is taken over all of the systematic uncertainties j. The η_{jk} are normalization scale factors, which are parametrized in terms of nuisance parameters α_j as follows:

$$\begin{aligned} \eta_{jk} \quad &\equiv \quad (1+\sigma_{jk})^{\alpha_j},\ \alpha \geq 0\,, \\ &\qquad\ (1-\sigma_{jk})^{-\alpha_j},\ \alpha < 0\,, \end{aligned} \tag{1}$$

where σ_{jk} is the uncertainty on component k due to systematic j, and α_j is a nuisance parameter with a Gaussian constraint of mean 0 and width 1. With this definition, η is always positive, and approaches $(1 + \alpha\,\sigma)$ for small $|\alpha|$.

The shape systematics are accounted for by introducing nuisance parameters α_j that describe how the nominal templates of sample k are distorted by the uncertainty j. This is done by defining, for every shape uncertainty and every sample, an "up" template $h^+_{jk}(x)$ and a "down" template $h^-_{jk}(x)$ obtained from

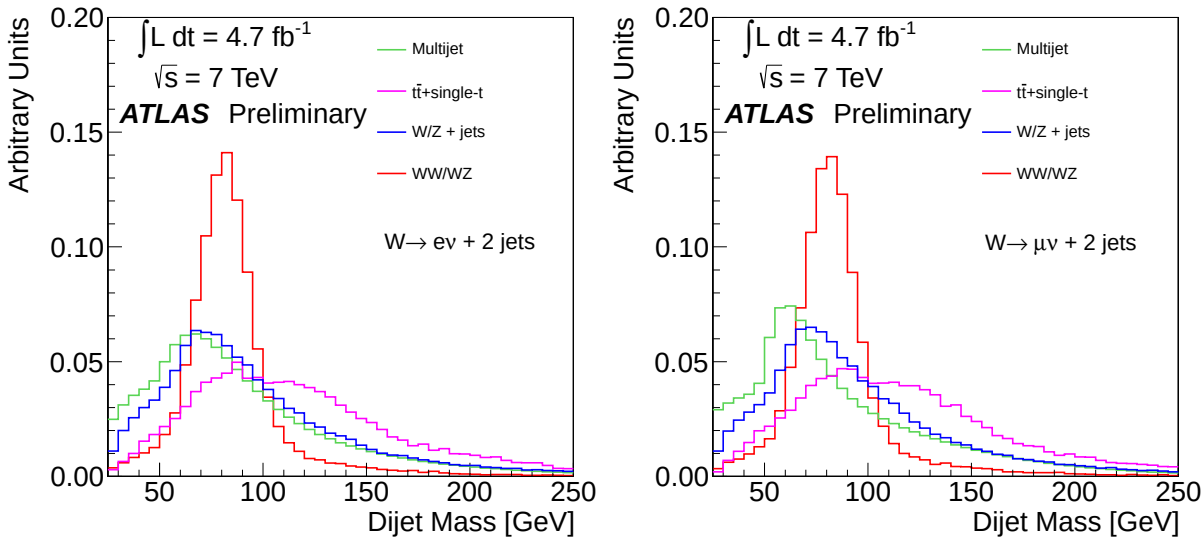

Figure 3: Nominal di-jet invariant mass templates of reconstructed $W/Z \rightarrow jj$ candidates for electron sample (left) and muon sample (right). The templates of $WW+WZ$, W/Z+jets and $t\bar{t}$, including single top production, are obtained from MC, while the multijet template is obtained from a data-driven method. All templates are normalized to unit area.

Table 2: Summary of the systematic sources considered and method to estimate their effect on the cross section measurement. The last column indicates which parameters are included in the likelihood definition (profiled) and which are estimated using pseudo-experiments.

Source of Systematic	Type	Profiled
W/Z+jets rate	Norm.	yes
W/Z+jet modeling	Shape	yes
$t\bar{t}$+single t rate	Norm.	yes
ISR/FSR for $t\bar{t}$	Norm. and Shape	yes
multijet rate	Norm.	no
multijet shape	Shape	no
PDF all processes but multijet	Norm.	no
JES uncertainty all processes but multijet	Shape	no
JES uncertainty signal	Norm.	no
JER uncertainty background except multijet	Shape	yes
JER uncertainty WW/WZ	Norm. and Shape	yes
lepton reconstruction all processes except multijet	Norm.	no
ISR/FSR for WW/WZ	Norm. and Shape	yes
MC statistics all processes	N.A.	no

varying the systematic uncertainty j by ± 1 sigma in sample k. A nuisance parameter α_j then parametrizes the shape variation systematic j according to:

$$\begin{aligned} h_{jk}(x) &= h^0_{jk}(x) + \alpha_j \left(h^+_{jk}(x) - h^0_{jk}(x) \right), \ \alpha_j \geq 0\,, \\ & \quad h^0_{jk}(x) - \alpha_j \left(h^-_{jk}(x) - h^0_{jk}(x) \right), \ \alpha_j < 0\,. \end{aligned} \tag{2}$$

If a particular uncertainty affects both shape and normalization the templates are not normalized and the variation of the nuisance parameter α_j results in a variation of both shape and normalization. The correlation between normalization and shape of all the systematic uncertainties considered in the fit is completely taken into account for the signal.

The systematic uncertainties in the electron and muon channels due to the same source are assumed to be 100 % correlated. However, uncertainties due to different sources are assumed to be mutually independent. The systematic uncertainties on the normalizations and shapes are included in the fit with Gaussian constraints, except for the jet energy scale and the multijet background uncertainties.

The jet energy scale shape systematic and multijet background uncertainty are not included in the likelihood fit. The systematic uncertainty is estimated by using a frequentist approach based on pseudo-experiments. In each pseudo-experiment the pseudo-data are generated based on randomly drawn values of the α_j for these systematic uncertainties, but fitted using the nominal values of α_j (i.e., zero). The rms of the signal cross section values observed in these pseudo-experiments is used to estimate the corresponding systematic uncertainty. The jet energy scale normalization systematic for the signal is taken into account by evaluating the yield variation of the WW/WZ samples when the scale is varied by ± 1 sigma. A summary table listing all the systematic sources affecting normalization and shape and how their effect on the cross section measurement is estimated is shown in Table 2.

The uncertainty due to the limited MC statistics used to create the templates is also estimated using pseudo-experiments. The pseudo-data are generated from templates whose bins are fluctuated according to their statistical uncertainty, and then fitted with the original templates.

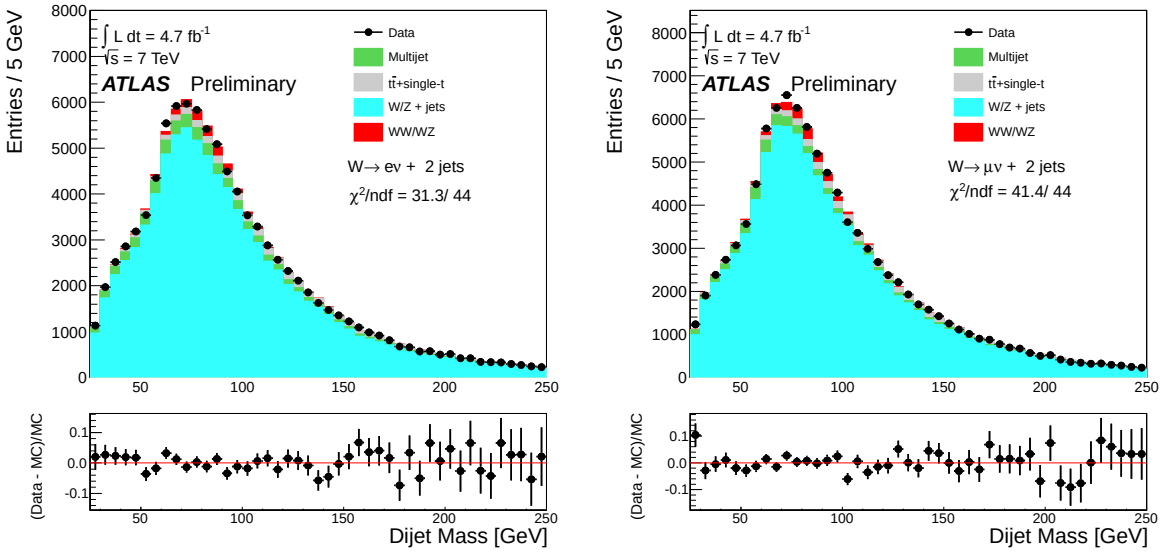

Figure 4: Di-jet invariant mass distribution of reconstructed $W/Z \to jj$ candidates for electron (left) and muon (right) channels, compared to the fitted signal and background components (top panel). The values of χ^2/ndf are also shown on the plots. The fractional difference between the data and the MC expectation as a function of m_{jj} for electron (let) and muon (right) channels are shown in the bottom panels.

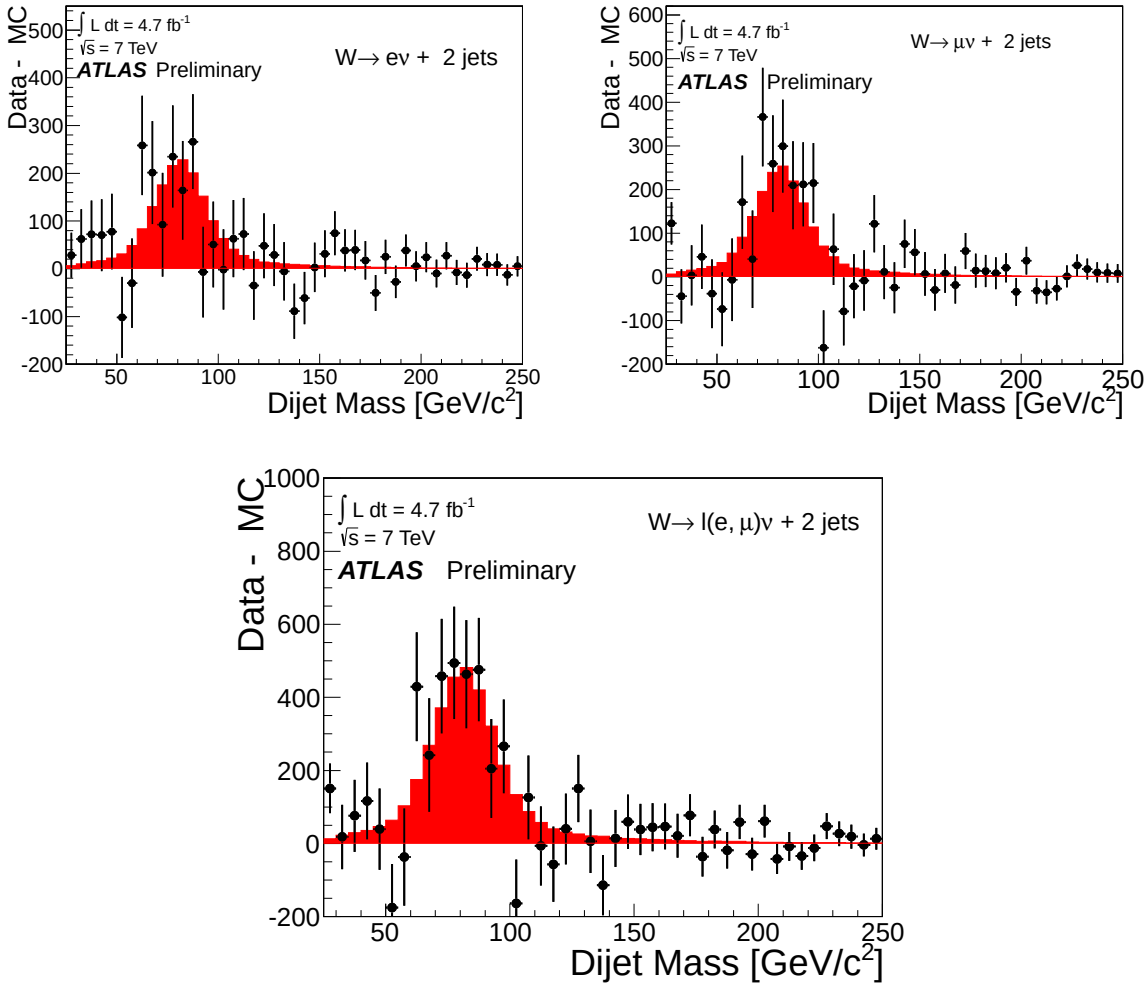

Figure 5: Background subtracted di-jet invariant mass distribution of reconstructed $W/Z \to jj$ candidates obtained for data (solid markers) for electron (top left) and muon (top right) channels and for the sum of the two channels (bottom). The errors bars represents statistical uncertainty of data and MC. The background prediction is obtained with the fitting procedure described in section 6. The expected di-jet invariant mass distributions from WW/WZ processes are shown as filled histograms.

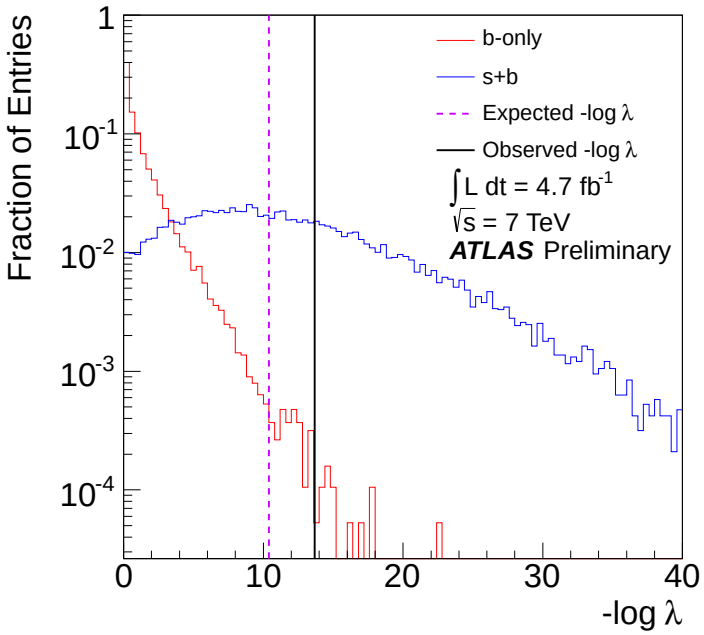

Figure 6: Distribution of the likelihood ratio λ, as defined in the text, for background-only (red line) and signal+background (blue line) pseudo-experiments. The expected value of λ for the signal+background hypothesis and the λ observed in data are also shown.

7 Results

Figure 4 shows the reconstructed di-jet invariant mass distribution in the electron and muon channels together with the fit results. The values of the χ^2/ndf for the fits in the electron and muon channels are 31.3/44 and 41.4/44 respectively. The signal MC m_{jj} distributions, normalized to the cross section extracted from the fit, are shown in Figure 5 together with the background subtracted data m_{jj} distribution for the electron (left) and muon (center) channels separately and for the two together.

The value of the ratio between the measured and the SM cross section obtained from the simultaneous fit to the di-jet invariant mass in electron and muon channels is $\mu = 1.13 \pm 0.34$, where the error is the quadratic sum of the systematic and statistical uncertainties. This leads to a measured $WW + WZ$ cross section equal to $\sigma(WW + WZ) = 72 \pm 9$ (stat.) $\pm$ 15 (syst.) $\pm$ 13 (MC stat.) pb. The individual contributions of each source of uncertainty to the cross section systematic uncertainty are listed in Table 3. The main contribution to the MC statistical uncertainty is due to the W+jets samples.

None of the nuisance parameters that are included in the likelihood are significantly pulled away from their input values. Most of them are not significantly constrained compared to their input values, except for those ones related to normalization and shape of W+jets that are further constrained due to the use of the full m_{jj} spectrum and the high statistics of the data sample.

The significance is estimated using the likelihood ratio λ, defined as the ratio between the maximum likelihood including the signal component in the fit, and the maximum likelihood with the signal fixed to zero. The expected significance is estimated to be 3.0 σ by performing pseudo-experiments generated according to the background-only and signal-plus-background hypotheses. The observed significance, including the effect of systematic uncertainties, is 3.3 σ. The distribution of the likelihood ratio for background-only and signal+background pseudo-experiments is shown in Figure 6.

Source	$\Delta\sigma/\sigma$[%]
Data Statistics	±12
MC Statistics	±18
W/Z+jets normalization	±11
W/Z jets shape variation	±5
Multijet shape and normalization	±5
Top normalization	±6
Top ISR/FSR	±1
Jet energy scale (all samples)	±12
Jet energy resolution (all samples)	±6
Lepton reconstruction (all samples)	±1
WW/WZ ISR/FSR	±2
JES uncertainty on WW/WZ normalization	±6
PDF (all samples)	±2
Luminosity	±3.9
Total systematics	±28

Table 3: Relative statistical and systematic uncertainty contributions (in %) to the total uncertainty on the measured signal cross-section σ_{WW+WZ}.

8 Conclusion

In summary, a search for a resonance consistent with the W or Z-boson was performed in the di-jet mass distribution in the lepton plus jets plus $E_{\mathrm{T}}^{\mathrm{miss}}$ final state. A resonance is observed with a significance of 3.3 standard deviations (σ), where 3.0 σ is expected. The observation is consistent with the SM production of the WW/WZ di-boson states. The WW + WZ cross section from a combination of the electron and muon leptonic W-decay channels is measured to be $\sigma(WW + WZ)$ = 72 ± 9 (stat.) ± 15 (syst.) ± 13 (MC stat.) pb, in good agreement with the prediction of 63.4 ± 2.6 pb from the SM. Measurements of these diboson processes are tests of the electroweak theory and a necessary step towards validating Higgs boson measurement techniques at the LHC.

References

[1] K. Hagiwara, S. Ishihara, R. Szalapski, and D. Zeppenfeld, *Low energy effects of new interactions in the electroweak boson sector*, Phys. Rev. D **48** (1993) 2182–2203.

[2] J. M. Campbell and R. K. Ellis, *An update on vector boson pair production at hadron colliders*, Phys. Rev. D **60** (1999) 113006.

[3] S. Frixione and B. R. Webber, *Matching NLO QCD computations and parton shower simulations*, JHEP **06** (2002) 029, `arXiv:hep-ph/0204244`.

[4] ATLAS Collaboration, *Measurement of W^+W^- production in pp collisions at $\sqrt{s}$ = 7 TeV with the ATLAS detector and limits on anomalous WWZ and WWγ couplings*, arXiv:1210.2979 [hep-ex], Submitted to Phys. Rev. **D**.

[5] ATLAS Collaboration, *Measurement of WZ production in proton-proton collisions at $\sqrt{s}$ = 7 TeV with the ATLAS detector* , arXiv:1208.1390 [hep-ex], Submitted to Eur. Phys. J. **C**.

[6] CMS Collaboration, *Measurement of WW production rate*, CMS-PAS-SMP-12-005.

[7] CMS Collaboration, *Measurement of the WW, WZ and ZZ cross sections at CMS*, CMS-PAS-EWK-11-010.

[8] CDF Collaboration, T. Aaltonen et al., *Measurement of the WW+WZ Production Cross Section Using the Lepton+Jets Final State at CDF II*, Phys.Rev.Lett. **104** (2010) 101801, arXiv:0911.4449 [hep-ex].

[9] D0 Collaboration, V. M. Abazov et al., *Measurements of WW and WZ production in W + jets final states in $p\bar{p}$ collisions*, Phys.Rev.Lett. **108** (2012) 181803, arXiv:1112.0536 [hep-ex].

[10] CMS Collaboration, *Measurement of the sum of WW and WZ production with W+dijet events in pp collisions at $\sqrt{s}$ = 7 TeV*, arXiv:1210.7544 [hep-ex], Submitted to Eur. Phys. J. **C**.

[11] ATLAS Collaboration, *Luminosity Determination in pp Collisions at sqrt(s) = 7 TeV using the ATLAS Detector in 2011*, ATLAS-CONF-2011-116.

[12] ATLAS Collaboration, *The ATLAS Experiment at the CERN Large Hadron Collider*, JINST **3** (2008) S08003.

[13] ATLAS Collaboration, *The ATLAS Simulation Infrastructure*, Eur.Phys.J. **C70** (2010) 823–874, arXiv:1005.4568 [physics.ins-det].

[14] S. Agostinelli et al., *GEANT 4, A Simulation Toolkit*, Nucl. Instrum. Meth. **A506** (2003) 250.

[15] M. L. Mangano, M. Moretti, F. Piccinini, R. Pittau, and A. Polosa, *ALPGEN, a generator for hard multiparton processes in hadronic collisions*, JHEP **0307** (2003), hep-ph/0206293.

[16] J. Pumplin, D. Stump, J. Huston, H. Lai, P. M. Nadolsky, et al., *New generation of parton distributions with uncertainties from global QCD analysis*, JHEP **0207** (2002) 012, arXiv:hep-ph/0201195.

[17] G. Corcella, I. Knowles, G. Marchesini, S. Moretti, K. Odagiri, P. Richardson, M. Seymour, and B. Webber, *HERWIG 6.5*, JHEP **0101** (2001) 010, hep-ph/0011363.

[18] J. Butterworth, J. R. Forshaw, and M. Seymour, *Multiparton interactions in photoproduction at HERA*, Z.Phys. **C72** (1996) 637–646, arXiv:hep-ph/9601371.

[19] K. Melnikov and F. Petriello, *Electroweak gauge boson production at hadron colliders through O(alpha(s)**2)*, Phys.Rev. **D74** (2006) 114017, arXiv:hep-ph/0609070.

[20] ATLAS Collaboration, *Measurement of the production cross section for W-bosons in association with jets in pp collisions at $\sqrt{s}$ = 7 TeV with the ATLAS detector*, Phys.Lett. **B698** (2011) 325–345, arXiv:1012.5382 [hep-ex].

[21] T. Gleisberg, S. Hoeche, F. Krauss, M. Schonherr, S. Schumann, et al., *Event generation with SHERPA 1.1*, JHEP **0902** (2009) 007, arXiv:0811.4622 [hep-ph].

[22] T. Sjostrand et al., *High-energy physics event generation with PYTHIA 6.1*, Comput. Phys. Commun. **135** (2001) 238–259, arXiv:hep-ph/0010017.

[23] A. Sherstnev and R. Thorne, *Parton Distributions for LO Generators*, Eur.Phys.J. **C55** (2008) 553–575, arXiv:0711.2473 [hep-ph].

[24] S. Frixione, P. Nason, and C. Oleari, *Matching NLO QCD computations with Parton Shower simulations: the POWHEG method*, JHEP **0711** (2007) 070, arXiv:0709.2092 [hep-ph].

[25] P. M. Nadolsky, H.-L. Lai, Q.-H. Cao, J. Huston, J. Pumplin, et al., *Implications of CTEQ global analysis for collider observables*, Phys.Rev. **D78** (2008) 013004, arXiv:0802.0007 [hep-ph].

[26] M. Aliev, H. Lacker, U. Langenfeld, S. Moch, P. Uwer, et al., *HATHOR: HAdronic Top and Heavy quarks crOss section calculatoR*, Comput.Phys.Commun. **182** (2011) 1034–1046, arXiv:1007.1327 [hep-ph].

[27] N. Kidonakis, *Next-to-next-to-leading-order collinear and soft gluon corrections for t-channel single top quark production*, Phys.Rev. **D83** (2011) 091503, arXiv:1103.2792 [hep-ph].

[28] N. Kidonakis, *NNLL resummation for s-channel single top quark production*, Phys.Rev. **D81** (2010) 054028, arXiv:1001.5034 [hep-ph].

[29] N. Kidonakis, *Two-loop soft anomalous dimensions for single top quark associated production with a W^- or H^-*, Phys.Rev. **D82** (2010) 054018, arXiv:1005.4451 [hep-ph].

[30] B. P. Kersevan and E. Richter-Was, *The Monte Carlo event generator AcerMC version 2.0 with interfaces to PYTHIA 6.2 and HERWIG 6.5*, arXiv:hep-ph/0405247 (2004).

[31] J. Campbell, K. Ellis, and C. Williams, *Vector Boson Pair Production at the LHC*, FERMILAB-PUB-11-182-T **000** (2011) 035, arXiv:1105.0020v1[hep-ph].

[32] A. Martin, W. Stirling, R. Thorne, and G. Watt, *Parton distributions for the LHC*, Eur. Phys. J. **C 63** (2009) 189, arXiv:0901.0002 [hep-ph].

[33] A. Martin, W. Stirling, R. Thorne, and G. Watt, *Uncertainties on α_s global PDF analyses and implications for predicted hadronic cross sections*, Eur. Phys. J. **C 64** (2009) 653, arXiv:0905.3531 [hep-ph].

[34] ATLAS Collaboration, *Electron performance measurements with the ATLAS detector using the 2010 LHC proton-proton collision data*, Eur. Phys. J. **C 72** (2012) 1909, arXiv:1110.3174 [hep-ex].

[35] ATLAS Collaboration, *Measurements of the electron and muon inclusive cross-sections in proton-proton collisions at $\sqrt{s}$ = 7 TeV with the ATLAS detector*, Phys.Lett. **B707** (2012) 438–458, arXiv:1109.0525 [hep-ex].

[36] M. Cacciari, G. P. Salam, and G. Soyez, *The anti-k_t jet clustering algorithm*, JHEP **0804** (2008) 063, arXiv:0802.1189 [hep-ph].

[37] ATLAS Collaboration, *Jet energy measurement with the ATLAS detector in proton-proton collisions at sqrt(s) = 7 TeV*, arXiv:1112.6426 [hep-ex].

[38] ATLAS Collaboration, *Performance of Missing Transverse Momentum Reconstruction in Proton-Proton Collisions at 7 TeV with ATLAS*, Eur.Phys.J. **C72** (2012) 1844, arXiv:1108.5602 [hep-ex].

[39] M. Cacciari, M. Czakon, M. Mangano, A. Mitov, and P. Nason, *Top-pair production at hadron colliders with next-to-next-to-leading logarithmic soft-gluon resummation*, Phys. Lett. B **710** (2012) 612–622.